Thermal Potential of a Twin-Screw Compressor as Thermoelectric Energy Harvesting Source

Claudia Savescu
Romanian Research and Development Institute for Gas Turbines COMOTI, Romania | Politehnica Bucharest, Romania
claudia.borzea@comoti.ro

Valentin Petrescu
Romanian Research and Development Institute for Gas Turbines COMOTI, Romania | Politehnica Bucharest, Romania
valentin.petrescu@comoti.ro

Daniel Comeaga
National University of Science and Technology, Politehnica Bucharest, Romania
daniel.comeaga@upb.ro

Razvan Carlanescu
Romanian Research and Development Institute for Gas Turbines COMOTI, Romania
razvan.carlanescu@comoti.ro

Mihaela Roman
Romanian Research and Development Institute for Gas Turbines COMOTI, Romania | Politehnica Bucharest, Romania
mihaela.roman@comoti.ro

Daniel Lale
Romanian Research and Development Institute for Gas Turbines COMOTI, Romania | Politehnica Bucharest, Romania
daniel.lale@comoti.ro

Andrei Mitru
Romanian Research and Development Institute for Gas Turbines COMOTI, Romania
andrei.mitru@comoti.ro (corresponding author)

Received: 19 October 2023 | Revised: 25 January 2024 | Accepted: 28 January 2024

 DOI: https://doi.org/10.48084/etasr.6417

ABSTRACT

This study evaluates the potential of a twin-screw compressor as a heat source to harness thermal energy. Thermoelectric generators are a feasible solution for microenergy harvesting from waste heat based on the Seebeck effect. Thermographic infrared images of the compressor were used to assess potential installation spots. The physical mounting of the thermoelectric modules must consider certain hindering aspects. At first, the compressor skid is subject to standards and authorizations for its components, leaving only a couple of spots for screw-mounted module installations. Another inconvenience is the bonds in any thermoelectric material causing them not to withstand lateral mechanical stress in other directions except the *c*-axis perpendicular to the layers. Therefore, vibration measurements have to be performed beforehand. Numerical simulations were conducted, relying on the acquired thermoelectric modules as well as on the temperature and vibration data measured on the compressor. The thermoelectric generators

studied are part of a multisource piezoelectric and thermoelectric energy harvesting system under research and development.

Keywords-thermoelectric generator; energy harvesting; waste heat; twin-screw compressor; thermographic imaging

I. INTRODUCTION

Waste heat is inherent in any industrial process and machinery that produces mechanical work. Almost half of the heat generated is wasted and often dissipated in the surrounding environment, thus limiting the efficiency of the system [1, 2]. Thermoelectric Generators (TEGs) [3] are considered a promising and feasible solution for energy harvesting applications from waste heat, under the condition that a temperature gradient is provided across the Thermoelectric Module (TEM). TEGs can generate electric power by converting temperature gradients (or differences) into electric energy, relying on the Seebeck effect, as opposed to the inverse Peltier effect that is used in Thermoelectric Coolers (TEC) and limits TEG efficiency. This alternative microenergy harvesting source has received increased research interest in the last two decades [4-11]. The maximum power output provided in [11] corresponds to approximately 200°C temperature differences, which is impossible to achieve in practical applications with industrial machinery and difficult to maintain even in the laboratory for a long time. To maintain the temperature difference for a longer period, it is necessary to ensure forced convection cooling of the cold side, which implies devices such as air fans or water circulation pumps, leading to higher power consumption than the TEGs would be able to produce. Most studies dealt with a theoretical analysis or assessed only one thermocouple, not a whole module with more coupled n-p semiconductor pairs [5, 6, 9, 12-14]. Simulations were usually conducted over a more or less arbitrary temperature range. In [15], the thermo-mechanical integrity and power-generation performance of BiTe TEGs were investigated with two pairs of thermocouples with rectangular, prism, and cylindrical legs at a temperature difference of 100°C in unconstrained mechanical conditions, numerically analyzing power output, conversion efficiencies, and thermal stresses on the legs. In [16], a TEG module with 127 thermocouples with different leg geometries was simulated in Ansys and analyzed under convective and isoflux boundary conditions, providing a copper heat sink to cool the cold side. In [17], an equivalent circuit model was developed in a SPICE program for the thermal and electrical design of thermoelectric-based systems. The model was exploited to obtain the electrical power output when the heat exchange between the hot and cold sources is not ideal, mainly because it is maximum with a load resistance matching the TEG's equivalent resistance, which is not just the electrical resistance but also depends on the thermal contact resistance. In [18], a coupled multiphysics simulation model was developed in Modelica/Dymola to ensure the TEGs' optimal thermal connection and find an optimal design and electrical connection for the energy harvesting system. The aim was to establish an optimal thermoelectric system for a given heat source and objectives. Finally, in [19], emergent thermoelectric materials were summarized and recent advances in energy harvesting from waste heat were discussed.

This study proposes a realistic approach on the thermal potential of screw compressors for thermoelectric energy harvesting. Using Finite Element Method (FEM) simulations, conducted in COMSOL Multiphysics, the expected voltage and power outputs of TEGs were evaluated by introducing the temperature ranges measured via infrared thermographic scanning. The vibration amplitudes of the compressor were also considered in a frequency domain study conducted to reveal the von Mises stress exerted on the TEG module. As far as is known, there is no study reporting mechanical stress induced by vibrating machinery.

II. COMPRESSOR THERMAL IMAGES

Thermographic images were taken with an infrared camera on a CU90G compressor on a test bench [20]. Figure 1 presents the skid with its main components. The thermal scans were obtained in November 2021, when atmospheric temperatures in Bucharest, Romania ranged from 10 to 18°C. This is confirmed by the lower limit captured by the thermal imager in the figures hereinafter. In the image processing software, the emissivity of 0.95 was set and the background temperature was considered 18°C as the ambient maximum. Figure 2 shows the temperatures recorded on the cast iron housing of the compressor. As can be observed, the maximum temperature (hot point) reached in the target area was 67.3°C on the compressor housing. The cold point was 17.3°C.

Fig. 1. Compressor skid within the test bed.

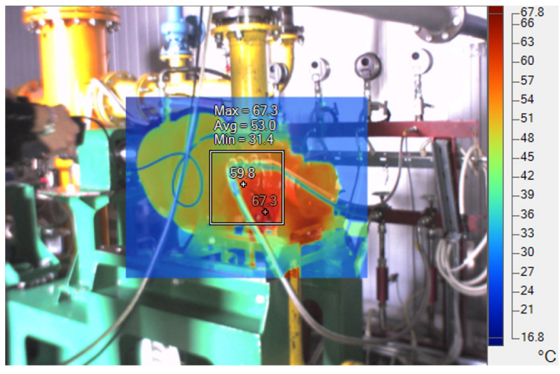

Fig. 2. Thermographic image of the compressor unit.

The compressor skid is subjected to regulations and standardizations, and drilling holes can render void its certifications. However, screw mounting with an applied torque of ~1.25 Nm per screw (0.128 kgm) is recommended [21] for satisfactory heat transfer, leaving only a couple of potential mounting places. The best option was the cover of the multiplier gearbox between the motor and the compressor (Figure 3 left), which is splashed with hot oil from within, making it ideal for this study's purposes. Figure 4 displays a thermographic image of the gearbox cover, showing a maximum temperature of 41.8°C.

Fig. 3. Optimal screw mounting spot for the TEGs.

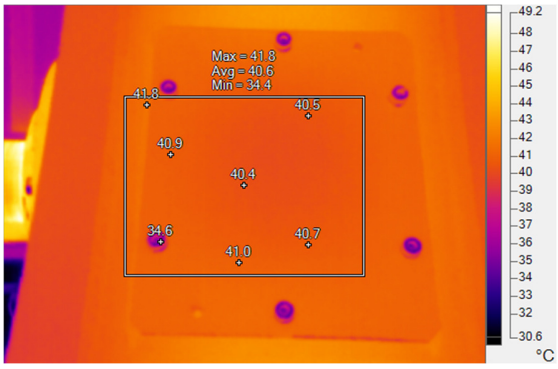

Fig. 4. Surface temperature range of the gearbox cover.

III. THERMOELECTRIC CONSIDERATIONS

Thermoelectric generators' efficiency depends on the temperature difference between the hot and cold sides, being related to the material's so-called figure of merit (zT), which depends on the material's conductivity according to:

$$zT = \frac{\varepsilon^2 \cdot \kappa_e \cdot T}{\kappa_d} \quad (1)$$

where zT [ND] is the figure of merit, ε [V/K] is the Seebeck coefficient, κ_e [1/Ωm] is the electrical conductivity, $T[K]$ is the temperature, and κ_d [W/mK] is the thermal conductivity. The Seebeck effect supposes a voltage being created across the TEM's sides, due to the temperature difference across a conductor or semiconductor. Two dissimilar (semi)conductors joined together represent a circuit's junctions. The A and B (semi)conductors are electrically connected in series and thermally in parallel. A junction is hot, with temperature T_{hot}, while the other one is cold, with temperature T_{cold}. The Seebeck voltage at the junctions of an open circuit is given by:

$$V = (\varepsilon_A - \varepsilon_B) \cdot (T_{hot} - T_{cold}) \Leftrightarrow \varepsilon_{AB} = \frac{V}{\Delta T} \quad (2)$$

where V [V] is the voltage, and ΔT [K] is the temperature difference. The thermoelectric modules require a very good contact for thermal transfer, most preferably with screw mounting. A spare cover was physically used to make holes and mount the thermoelectric harvesting components, as depicted in Figure 5. The original cover will be replaced in the upcoming experiments.

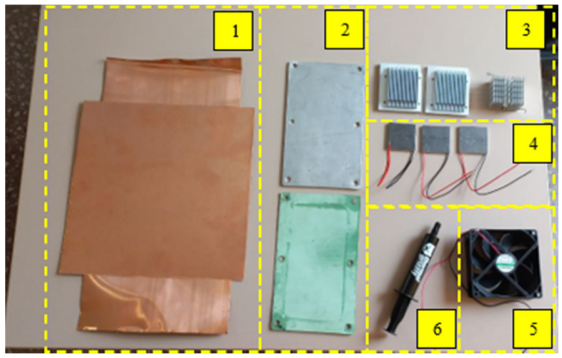

Fig. 5. Materials required for experiment: (1) Copper sheets for hot side contact; (2) Executed aluminum cover and sheet for sealing gasket; (3) Heat sinks; (4) Thermoelectric modules; (5) Fan; (6) Thermally conductive paste.

IV. SIMULATION MODEL

FEM simulations were performed in the COMSOL Multiphysics® software [22] using a multiphysics approach for a complete evaluation of both heat transfer and electric field problems. The simulation model was designed in an application builder, fully parametrized for thermoelectric coolers (TECs) [23], easing the geometry design for thermoelectric devices in general. The thermoelectric legs were assigned bismuth telluride (Bi_2Te_3) material of n-type and p-type, copper was used for the connection electrodes, and alumina ceramic was utilized for the plates acting as hot and cold sides. The overall dimensions of the chosen and subsequently acquired devices, of 40×40×5 [mm] [11] were considered in the simulation model. Detailed constructive elements and parameters are provided in [13]. The following physics were coupled in the simulation model:

- **Heat Transfer in Solids** to numerically model the heat transfer. In solid domains, the temperature equation corresponds to the differential form of the Fourier law and may present additional factors, such as heat sources [12]. The general formulas employed in the simulation software are:

$$\rho C_p \mathbf{u} \cdot \nabla T + \nabla \cdot \mathbf{q} = Q + Q_{ted}$$
$$\mathbf{q} = -k \nabla T \quad (3)$$

where ρ [kg/m^3] is the density, C_p [J/(kgK)] is the specific heat, $\mathbf{u}$ is the temperature T [K] or the electric potential V [V], Q [J] is the heat source, $k \mid \kappa_d$ [W/(m·K)] is the thermal conductivity, Q_{ted} [ND] is the thermoelastic dissipation

quality factor, and **q** [W/m^2] is the conduction heat flux. A temperature T1 of 30°C was declared for the cold side, and a temperature T2 of 80°C was initially set for the hot side, as exhibited in Figure 6.

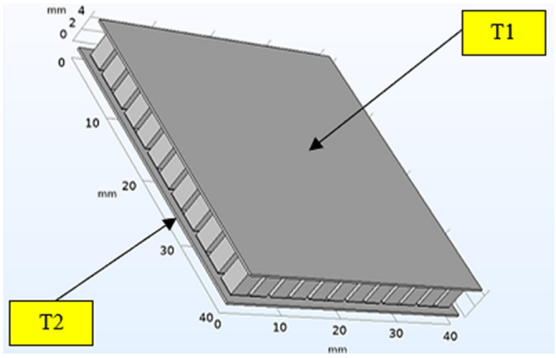

Fig. 6. TEG geometry and boundary conditions in heat transfer.

- **Electric Currents**: this physics interface, relying on Ohm's law, solves the equations for current conservation, considering the scalar value of the electric potential as a dependent variable. It is used for computing electric field, current, and electric potential distributions within conducting materials [12]. A reference impedance of 50 Ω is set by default in the simulation program,, and the current conservation condition was applied to the Bi_2Te_3 elements with the initial value of voltage $V = 0$ V.

$$\nabla \cdot \mathbf{J} = Q_{j,v}$$
$$\mathbf{J} = \sigma\mathbf{E} + \mathbf{J_e} \quad (4)$$
$$\mathbf{E} = -\nabla V$$

where **J** [A] is the electric current, $Q_{j,v}$ [A] is the current source, σ | κ_e [S/m] is the electric conductivity, **E** [V/M] is the electric field, $\mathbf{J_e}$ [A] is the external current source, and V [V] is the electric potential. Ground (GND) and Floating Potential (FP) boundary conditions were applied, as in Figure 7, on the back surfaces in contact with the hot side of the module.

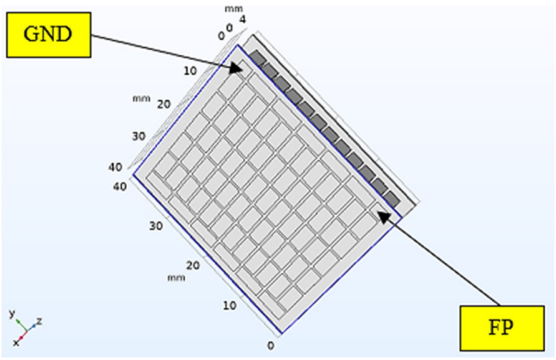

Fig. 7. TEG geometry showing the electric boundary conditions.

- **Thermoelectric Effect** multiphysics interface links together geat transfer in solids and electric currents' physics interfaces for a complete modeling of Peltier-Seebeck-Thomson thermoelectric effects, solving the equation system for a complete evaluation of both thermal and electrical parameters describing the multiphysics interrelations [12]:

$$P = ST$$
$$\mathbf{q} = P\mathbf{J} \quad (5)$$
$$\mathbf{J_e} = -\sigma S \nabla T$$

where P | π [V] is the Peltier coefficient, S | ε [V/K] is the Seebeck coefficient, T [K] is the temperature, **q** [W/m^2] is the conduction heat flux, **J** [A] is the induced electric current, $\mathbf{J_e}$ [A] is the external current source, and σ | κ_e [S/m] is the electric conductivity. It is worth providing the main properties of the bismuth telluride material used by the simulation program (assumed the same for n- and p-type), as shown in Table I.

TABLE I. PROPERTIES OF BISMUTH TELLURIDE MATERIAL

T [K]	S [V/K]	k [W/m/K]	σ [S/m]
200	168e-6	24e-1	1.4286e5
250	192e-6	19e-1	1.1111e5
300	210e-6	16e-1	0.86957e5
350	225e-6	16e-1	0.71429e5
400	237e-6	17.5e-1	0.58824e5

- **Electromagnetic Heating** multiphysics coupling adds the source term for resistive (ohmic) heating, Qe [W/m^3] as:

$$\rho C_p \frac{\partial T}{\partial t} - \nabla \cdot (k\nabla T) = Q_e \quad (6)$$

where ρ [kg/m^3] is density, C_p [J/(kgK)] is the specific heat, T [K] is the temperature, t [s] is the time, k | κ_d [W/(m·K)] is the thermal conductivity, and Q_e [W/m3] is the resistive heating.

- **Electrical Circuit** is an extra physics interface that needs to be added when connecting external circuit components. A 2.4 kΩ load resistor was connected in parallel to obtain current and power information besides voltage. This value was not randomly chosen but represents the power required by the wireless sensor nodes [24], which need to be powered within the practical application using microenergy harvesting devices.

- **Solid Mechanics** was added to account for the vibration speeds on all axes, as measured on the CU90G compressor driven at 2500 rpm [25]. The boundary selected was the exterior hot side surface, the same as T2 (Figure 6). The input values are provided in Table II.

TABLE II. PRESCRIBED VELOCITY

Direction	Symbol	Value [U.M.]
Prescribed on x direction	v_x	0.998 [mm/s]
Prescribed on y direction	v_y	2.985 [mm/s]
Prescribed on z direction	v_z	1.692 [mm/s]

Solid Mechanics physics interface requires filling in additional material properties for Bismuth Telluride, namely Young's modulus (E) and Poisson's ratio (ν). Since these

characteristics are not given by the manufacturer, E was set to 32 GPa and ν was set to 0.25, as found in [26].

V. RESULTS AND DISCUSSION

A. Stationary Study - Thermal and Electrical Evaluation

A stationary study was conducted to assess the thermoelectric parameters. A parametric sweep for T_{hot}, range(40,5,80) degC, was set in to grasp the influence of the temperature difference on the electric output. Figure 8 shows the temperature gradient, from 30 to 80°C, across the thermoelectric module. The direction of the conductive heat flux is represented by arrows (from the hot side towards the cold side). Figure 9 portrays the electric potential. TEGs' voltage output is in VDC, hence the variation is from 0 V on the boundary where the ground condition was applied, to the maximum value of 1.55 V a temperature difference of 50°C, on the boundary declared with floating potential. If the floating potential is connected to a circuit or a value for electric current is set, this one acts like a terminal.

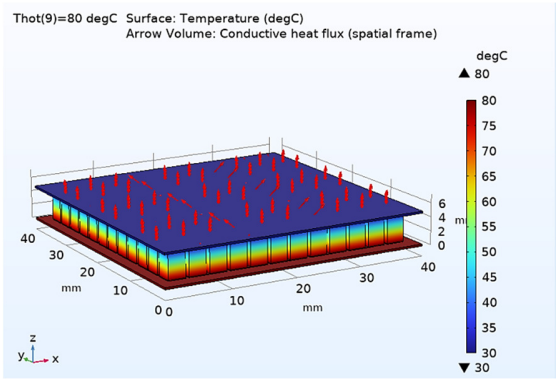

Fig. 8. Temperature gradient across the thermoelectric module.

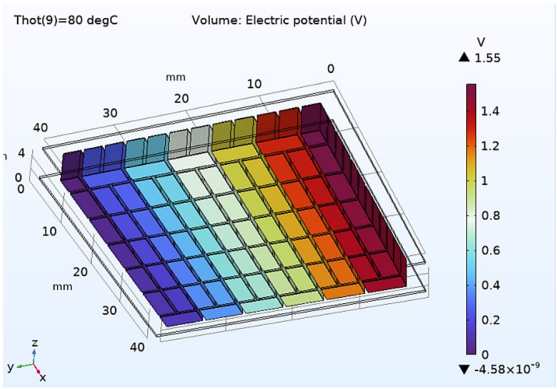

Fig. 9. Electric potential evaluation for hot side temperature of 80 °C.

Figure 10 demonstrates the voltage, current, and power curves for the hot side temperature. Secondary (right) axis values correspond to current [mA] and power [mW]. The evaluation was carried out on the load resistance of 2.4 kΩ. Figure 11 displays the current-voltage and current-power curves plotted in the simulation software. A linear current-voltage dependence indicates the correctness of the result trends, as well as the current-power curve.

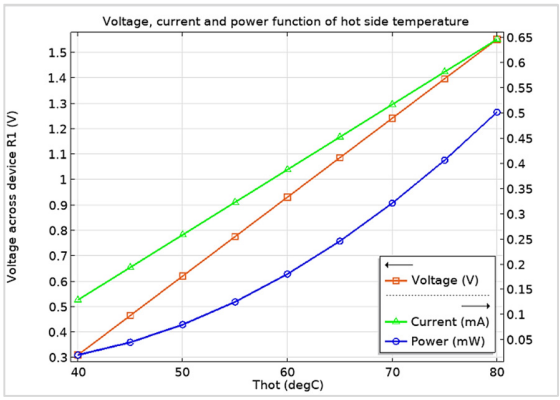

Fig. 10. Voltage, current, and power to load resistor, function of T_{hot}.

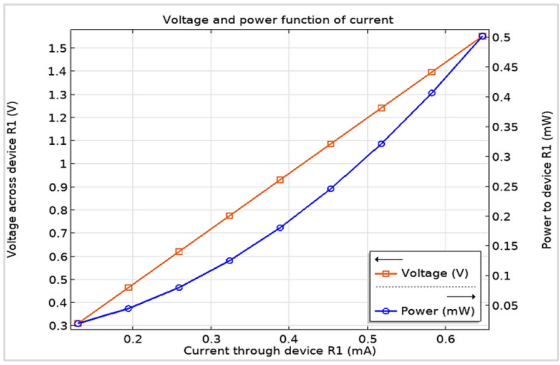

Fig. 11. Voltage and power function of current through resistor.

B. Frequency Domain Study – Stress Evaluation

Regarding the following stress evaluation [27], it should be noted that the crystal structure of Bi_2Te_3 consists of a hexahedral-layered structure with five atomic layers, a so-called quintuple ($Te^{(1)}$–Bi–$Te^{(2)}$–Bi–$Te^{(1)}$). Bonds within the quintuple are covalent, but between the $Te^{(1)}$ tellurium planes of adjacent quintuples there are weak van der Waals interactions along the c-axis of the unit cell, thus presenting an increased susceptibility to breakdown [23-24]. Figure 12 shows that the maximum stress value is 0.759 kPa, much less than the supported compression stress of 62 MPa declared in [26] for the same Bi_2Te_3 material.

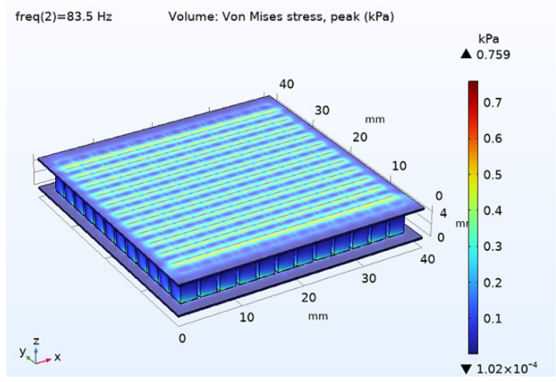

Fig. 12. Von Mises stress peak evaluation at 83.5 Hz.

The physical application involves sinusoidal vibration waves, hence the stress evaluation addresses the von Mises stresses in a frequency domain study, where everything is considered sinusoidal. The compressor does not yield any lateral linear forces on the TEG modules within its normal operation. The vibrational behavior of the rotary-bladed machinery does not present any risk to the thermoelectric modules' yield strength. The measured male rotor frequency of 83.5 Hz was considered for this purpose, due to the highest vibration amplitudes exhibited [25].

VI. CONCLUSIONS

This paper presents a realistic simulation model and results for the application of harvesting waste heat from a twin-screw compressor. All boundary loads considered in the numerical simulations are real data measured on the compressor and the model relied on physical TEGs. A frequency domain study revealed that the compressor's vibrations on all axes do not present a risk to damage the TEM and it is therefore safe to use in this application, since the compressor only produces sinusoidal vibration waves. The stationary study showed very pertinent results, comparable to the plots in the product specifications. The curves obtained for current, voltage, and power validated the correctness of the simulation model. This study did not aim to model an ideal heat source to obtain high values of thermoelectric power, as most studies in the literature, but to assess what could be practically expected from the harvesting of industrial waste heat. Consequently, the values of the electric parameters are insufficient to power wireless sensor nodes in terms of voltage output. Thermoelectric generators have been envisaged as a backup source for a multisource energy harvesting system, primarily based on piezoelectric harvesting from vibrations. Multiple harvesters must be electrically connected to meet the power requirements of the sensor nodes.

So far, no studies have been reported to apply mechanical vibrations in the simulation to assess von Mises stress in a frequency domain study along with classical TEG stationary studies. Furthermore, both the vibration and temperature data introduced in the simulation model were measured on an industrial compressor test bench. Future research will pursue conducting experimental tests, and adding a heatsink in the simulation model to compare to the physical model for proper result validation.

ACKNOWLEDGMENT

This study is part of the "Nucleu" program within the Romanian Research, Development, and Innovation Plan 2022-2027, conducted with the support of the Romanian Ministry of Research, Innovation, and Digitalization, contract 31N/2023, project number PN 23.12.09.

REFERENCES

[1] H. Jouhara, N. Khordehgah, S. Almahmoud, B. Delpech, A. Chauhan, and S. A. Tassou, "Waste heat recovery technologies and applications," *Thermal Science and Engineering Progress*, vol. 6, pp. 268–289, Jun. 2018, https://doi.org/10.1016/j.tsep.2018.04.017.

[2] K. R. Artoni, Ang, I. Yamazaki, K. Hirata, S. Singh, M. Matsunami, and T. Takeuchi, "Development of Cu2Se/Ag2(S,Se)-Based Monolithic Thermoelectric Generators for Low-Grade Waste Heat Energy Harvesting," *ACS Applied Materials & Interfaces*, vol. 15, no. 40, pp. 46962–46970, Oct. 2023, https://doi.org/10.1021/acsami.3c09823.

[3] B. Safaei, S. Erdem, M. Karimzadeh Kolamroudi, and S. Arman, "State-of-the-art review of energy harvesting applications by using thermoelectric generators," *Mechanics of Advanced Materials and Structures*, 2023, https://doi.org/10.1080/15376494.2023.2217660.

[4] K. S. Ong, L. Jiang, and K. C. Lai, "Thermoelectric Energy Conversion," vol. 4, I. Dincer, Ed. Oxford, UK: Elsevier, 2018, pp. 794–815.

[5] B. Buonomo, F. Cascetta, A. di Pasqua, C. Fiorito, and O. Manca, "Numerical investigation on a thermoelectric generator in an exhaust automotive line with convergent metal foam," *Journal of Physics: Conference Series*, vol. 2385, no. 1, Sep. 2022, Art. no. 012057, https://doi.org/10.1088/1742-6596/2385/1/012057.

[6] Y. J. Cui, B. L. Wang, and K. F. Wang, "Thermally induced vibration and strength failure analysis of thermoelectric generators," *Applied Thermal Engineering*, vol. 160, Sep. 2019, Art. no. 113991, https://doi.org/10.1016/j.applthermaleng.2019.113991.

[7] A. Gürcan and G. Yakar, "Investigation of the performance of a thermoelectric generator system utilizing the thermal energy of air compressed in a compressor," *Journal of the Korean Physical Society*, vol. 80, no. 6, pp. 467–483, Mar. 2022, https://doi.org/10.1007/s40042-022-00425-x.

[8] Z. Varga and E. Rácz, "Experimental Investigation of the Performance of a Thermoelectric Generator," in *2022 IEEE 20th Jubilee World Symposium on Applied Machine Intelligence and Informatics (SAMI)*, Poprad, Slovakia, Mar. 2022, pp. 000159–000164, https://doi.org/10.1109/SAMI54271.2022.9780741.

[9] J. H. Meng, X. X. Zhang, and X. D. Wang, "Multi-objective and multi-parameter optimization of a thermoelectric generator module," *Energy*, vol. 71, pp. 367–376, Jul. 2014, https://doi.org/10.1016/j.energy.2014.04.082.

[10] M. N. Hanani, J. Sampe, J. Jaffar, and N. H. M. Yunus, "Development of a Hybrid Solar and Waste Heat Thermal Energy Harvesting System," *Engineering, Technology & Applied Science Research*, vol. 13, no. 3, pp. 10680–10684, Jun. 2023, https://doi.org/10.48084/etasr.5561.

[11] "TEGpro TE-MOD10W4V-40," TEGpro, Sep. 2014. [Online]. Available: https://www.tegmart.com/datasheets/TGPR-10W4V-40S.pdf.

[12] A. Prasad and R. C. N. Thiagarajan, "Multiphysics Modelling and Multilevel Optimization of Thermoelectric Generator for Waste Heat Recovery," 2018. [Online]. Available: https://www.comsol.com/paper/multiphysics-modeling-and-development-of-thermoelectric-generator-for-waste-heat-61281.

[13] C. Săvescu, A. Morega, Y. Veli, and V. Petrescu, "Numerical Modelling of Thermoelectric Energy Harvesting from Industrial Compressor Waste Heat," in *2023 13th International Symposium on Advanced Topics in Electrical Engineering (ATEE)*, Bucharest, Romania, Mar. 2023, pp. 1–6, https://doi.org/10.1109/ATEE58038.2023.10108390.

[14] N. Jaswanth and G. RaamDheep, "Thermoelectric maximum power point tracking by artificial neural networks," *Soft Computing*, vol. 27, no. 7, pp. 4041–4050, Apr. 2023, https://doi.org/10.1007/s00500-023-07948-w.

[15] U. Erturun, K. Erermis, and K. Mossi, "Influence of leg sizing and spacing on power generation and thermal stresses of thermoelectric devices," *Applied Energy*, vol. 159, pp. 19–27, Dec. 2015, https://doi.org/10.1016/j.apenergy.2015.08.112.

[16] C. Maduabuchi and R. Lamba, "Photovoltaic-Thermoelectric Power Generation: Effects of Photovoltaic Cell Type, Thermoelectric Leg Geometry, and Multistaging on System Performance," in *Sustainable Energy Storage for Furthering Renewable Energy*, Begell House, 2022.

[17] G. Pennelli, E. Dimaggio, and M. Macucci, "Electrical and thermal optimization of energy-conversion systems based on thermoelectric generators," *Energy*, vol. 240, Feb. 2022, Art. no. 122494, https://doi.org/10.1016/j.energy.2021.122494.

[18] M. Nesarajah and G. Frey, "Multiphysics Simulation in the Development of Thermoelectric Energy Harvesting Systems," *Journal of Electronic Materials*, vol. 45, no. 3, pp. 1408–1411, Mar. 2016, https://doi.org/10.1007/s11664-015-4049-1.

[19] S. Singh, K. Hirata, S. K. Pandey, and T. Takeuchi, "Recent Advances in Energy Harvesting from Waste Heat Using Emergent Thermoelectric Materials," in *Emerging Materials: Design, Characterization and Applications*, L. R. Thoutam, S. Tayal, and J. Ajayan, Eds. Singapore: Springer Nature, 2022, pp. 155–184.

[20] "COMOTI – Institutul National de Cercetare Dezvoltare Turbomotoare." https://comoti.ro/en/home-2/.

[21] "TEGpro: Module Installation Notes," TEGpro. [Online]. Available: https://www.tegmart.com/datasheets/TGPR-MOD-INST.pdf.

[22] "COMSOL Multiphysics® Software - Understand, Predict, and Optimize," *COMSOL*. https://www.comsol.com/comsol-multiphysics.

[23] "Thermoelectric Cooler," *COMSOL*. https://www.comsol.com/model/thermoelectric-cooler-30611.

[24] "LTC3588-2 - Nanopower Energy Harvesting Power Supply with 14V Minimum VIN," Linear Technology. [Online]. Available: https://www.analog.com/media/en/technical-documentation/data-sheets/35882fc.pdf.

[25] C. Borzea, V. Petrescu, I. Vlăducă, M. Roman, and G. Badea, "Potential of Twin-Screw Compressor as VIbration Source for Energy Harvesting Applications," *Electrical Machines, Materials and Drives*, vol. 17, no. 1, pp. 91–96, 2021.

[26] G. M. Guttmann, Y. Gelbstein, G. M. Guttmann, and Y. Gelbstein, "Mechanical Properties of Thermoelectric Materials for Practical Applications," in *Bringing Thermoelectricity into Reality*, IntechOpen, 2018.

[27] F. Khelil, M. Belhouari, N. Benseddiq, and A. Talha, "A Numerical Approach for the Determination of Mode I Stress Intensity Factors in PMMA Materials," *Engineering, Technology & Applied Science Research*, vol. 4, no. 3, pp. 644–648, Jun. 2014, https://doi.org/10.48084/etasr.442.

[28] D. Teweldebrhan, V. Goyal, and A. A. Balandin, "Exfoliation and Characterization of Bismuth Telluride Atomic Quintuples and Quasi-Two-Dimensional Crystals," *Nano Letters*, vol. 10, no. 4, pp. 1209–1218, Apr. 2010, https://doi.org/10.1021/nl903590b.

[29] T. Nehari, A. Ziadi, D. Ouinas, and B. Boutabout, "Numerical Study of the Effect of the Penetration of a Crack in the Matrix of a Composite," *Engineering, Technology & Applied Science Research*, vol. 4, no. 3, pp. 649–655, Jun. 2014, https://doi.org/10.48084/etasr.447.